Effect of epitaxial strain on the exchange-bias properties of $[La_{0.67}Ca_{0.33}MnO_3/La_{0.33}Ca_{0.67}MnO_3]_{15}$ multilayers: Resonant x-ray scattering measurements

C. Christides*
Department of Engineering Sciences, School of Engineering, University of Patras, 26504 Patras, Greece and Department of Chemistry, University of Durham, Durham DH1 3LE, United Kingdom

P. P. Deen
Institut Laue Langevin, 6 Rue Jules Horowitz, Boîte Postale 156, 38042 Grenoble Cedex, France

N. Moutis
Institute of Materials Science, NCSR Demokritos, 15310 Athens, Greece

E. Houssakou
Department of Engineering Sciences, School of Engineering, University of Patras, 26504 Patras, Greece

L. Bouchenoire
XMaS CRG, ESRF, Boîte Postale 220, 38043 Grenoble Cedex, France

K. Prassides
Department of Chemistry, University of Durham, Durham DH1 3LE, United Kingdom

(Received 14 April 2006; revised manuscript received 30 November 2006; published 25 January 2007)

Complementary x-ray synchrotron radiation diffraction (XRD) and resonant scattering (RXS) measurements were performed at the Mn *K*-edge between 10 and 300 K in order to analyze the effect of epitaxial strain and tetragonal lattice distortions on the exchange bias (EB) mechanism observed in $[La_{2/3}Ca_{1/3}MnO_3(FM)/La_{1/3}Ca_{2/3}MnO_3(AF)]_{15}$ multilayers below a blocking temperature, T_B, of 80 K. XRD measurements showed that the c/a axial ratio, an indication of the tetragonal lattice distortion in pseudocubic lattice settings, reaches its maximum at the onset of the EB effect and the corresponding structural correlation length varies substantially at the onset of T_B. The in-plane lattice parameter a at T_B is close to the bulk lattice parameters of the antiferromagnetic (AF) layers, thus indicating that the EB effect is related with the accommodation of strain inside the ferromagnetic (FM) and AF layers. RXS measurements revealed a ferrodistortive (FD) state. The RXS intensity difference signal exhibits a main-edge feature and a postedge feature at ~6.57 keV that scales linearly with temperature and the c/a ratio up to 80 K. The disappearance of the postedge feature above 80 K($=T_B$) may signify a rearrangement of Mn-O-Mn bonding angles due to strain-driven effects at the FM/AF interfaces, inducing disorder in FD octahedral tilt ordering which may pin the local distortions below the T_B.

DOI: 10.1103/PhysRevB.75.014432 PACS number(s): 75.47.Lx, 41.60.Ap, 68.65.Ac, 61.10.−i

I. INTRODUCTION

The exchange bias (EB) phenomenon has received considerable attention because of its important applications in magnetic storage devices.[1] Of particular interest are the EB properties of colossal magnetoresistance (CMR) compositionally modulated structures consisting of antiferromagnetic (AF) and ferromagnetic (FM) (La,Ca)MnO_3 layers[2,3] because manganites are strongly correlated electron systems, in which the magnetic, electronic and crystal structures interact strongly with each other. The existence of EB was revealed[2] at first in $[La_{2/3}Ca_{1/3}MnO_3(FM)/La_{1/3}Ca_{2/3}MnO_3(AF)]_{15}$ multilayers. Systematic studies[2–4] have shown that EB appears below a blocking temperature T_B of about 80 K, which is smaller than the charge-ordering (CO) ($T_{CO} \approx 250$ K) and the Néel ($T_N \approx 140$ K) temperatures[5] of the AF layers. It is now accepted that[3,4] the EB effects in these multilayers are strongly related to the steep decrease of the field-cooled magnetization, M_{FC} and the FC resistivity between 5 and 80 K. T_B is independent[3] of the thickness of the AF and FM layers, the Ca^{2+}concentration and the Mn^{3+}:Mn^{4+} interface ratio. Electron microscopy and x-ray diffraction measurements [4] indicate that the EB properties are sensitive to local crystal structural properties and the strain fields induced by the lattice mismatch between the AF and FM layers. Our aim is to explore the importance of lattice distortions on the elusive EB mechanism in $[La_{2/3}Ca_{1/3}MnO_3(FM)/La_{1/3}Ca_{2/3}MnO_3(AF)]_{15}$ multilayers.

Resonant x-ray scattering (RXS) near the Mn *K*-edge has proven to be a powerful experimental tool that probes the distortion of the MnO_6 octahedral sites[6–8] in the parent $LaMnO_3$ compound of CMR materials. In the case of nonmagnetic RXS, incident x-rays, tuned around the *K*-edge of Mn^{3+}, cause a dipole transition from the $1s$ orbital to the $4p_i$ ($i=x,y,z$) orbital. Subsequently, the $4p_i$ electron recombines with the core hole by emitting an x-ray photon with an energy equal to the incident one. Thus, this transition itself does not directly access the $3d$-orbitals. In $La^{3+}Mn^{3+}O_3^{2-}$, the

MnO_6 octahedra are not only tilted by the $GdFeO_3$-type of distortion[9,10] but, in view of the $t_{2g}^3 e_g^1 (3d^4)$ configuration of the Mn^{3+} ion, are Jahn-Teller (JT) distorted by the basal-plane distortion mode[11–13] Q_2. Cooperative JT ordering of Q_2-distorted MnO_6 octahedra[13] results in antiferrodistortive (AFD) ordering[6,14] that reduces the elastic energy of $LaMnO_3$. Band structure calculations[15,16] indicate that the dipolar RXS spectra are a direct reflection of *lattice distortions*, since the Mn $4p_i$-state in the intermediate excited state is influenced by lattice distortions through hybridization with the $2p$-states of neighboring oxygen sites.

In addition, the e_g-orbital degrees of freedom are coupled to lattice distortions via the exchange coupling (double-exchange or super-exchange) mechanisms,[13] which involve the $2p$-orbital states at oxygen sites along Mn-O-Mn bonds. Thus, earlier RXS experiments have considered[6,18] that resonant scattering at the Mn K-edge reflects the symmetry of the orbital ordering via the redistribution of local charge density (and subsequent perturbation of the electronic levels) at the Mn^{3+} sites. In the JT-distorted[6,8] $LaMnO_3$, the periodicity of the Mn orbital ordering is the same as that of the octahedral tilt ordering. However, the periodicity of the Mn orbital order is not the same as that of the octahedral tilt order in at least some hole-doped $R^{3+}_{1-x}M^{2+}_{1-x}Mn^{3+}_{x}Mn^{4+}_{1-x}O_3$ manganites, such as[17–19] $Pr_{1-x}Ca_xMnO_3$. Since substitution of R^{3+} by M^{2+} ions introduces JT-inactive Mn^{4+} ions, hole hopping is expected to turn a JT-active Mn^{3+} site into a JT-inactive Mn^{4+} site. Thus, the movement of a hole is accompanied by the movement of a lattice distortion (dressed hole). If these hole-doped manganites undergo a charge-ordering (CO) transition, then all the Mn^{3+} sites may exhibit a cooperative JT distortion[11,20] due to regular ordering of local (static) JT distortions below the transition temperature T_{CO}. It is worth emphasizing the difference of the AFD state between the parent $LaMnO_3$ structure and the hole-doped CO manganites. AFD ordering of $Mn^{3+}O_6$ octahedra takes place in $LaMnO_3$ because the minimization of elastic energy of the lattice is in favor[12] of a Q_2 JT-active mode only. Thus, strong Mn K-edge dipolar RXS signals were observed[6] at the orbital-order superlattice reflections (with integer Miller indices) that coincide with the reflections from the AFD supercell, since there are no $Mn^{4+}O_6$ octahedral sites. In half doped manganites,[21] such as $Nd_{0.5}Sr_{0.5}MnO_3$, resonant CO and AFD-ordering reflections were observed for integer and half-integer Miller indices, respectively, indicating that the AFD supercell is doubled along the specific lattice directions relative to the CO superlattice. These RXS results have been interpreted[21] by assuming the presence of tetragonally distorted and regular octahedral MnO_6 sites. Other (of non-RXS-type) measurements[22] have provided indirect evidence for the role of the cooperative JT distortions on the stability of the CO state in $La_{1-x}Ca_xMnO_3$ ($0.5 \leqq x \leqq 0.9$) manganites, indicating that an increasing (decreasing) fraction of the octahedral stretching Q_3 (basal-plane tetragonal Q_2) mode, first, stabilizes the CO state, and second, evolves with the types of magnetic ordering observed as x increases. These effects indicate that a CO transition affects the E_g-type octahedral distortions, referred to as Q_2 and Q_3 strain modes, by influencing the cooperative JT distortions in the lattice (and *vice versa*).

Although Mn K-edge (dipolar) RXS measurements *cannot* probe the level splitting of t_{2g}- and e_g-states for E_g-type octahedral distortions, they can probe both, the AFD ordering of MnO_6 octahedra via the polarization anisotropy of the complex x-ray atomic scattering factors (ASF), and the coherent modulation length of CO and AFD-ordering regions from the peak width of resonant reflections.[17] Based on these principles, RXS experiments were able to probe the variation of MnO_6 distortions induced by epitaxial strain in thin films[23,24] and multilayers[25] of manganites. These studies[23–25] have analyzed the RXS results by considering JT distortions despite the fact[24] that the situation is more complex and that tetragonal lattice distortions induced by epitaxial strain (extrinsic effect) should not be confused with JT modes (intrinsic effect) of tetragonal Q_2 and Q_3 distortions.[11,26] Tetragonal distortions can be induced in perovskite manganite thin films from the heterojunctions between the lattice mismatched manganites and the substrates, which force the films to match their in-plane lattice parameter to that of the substrate. Dipolar RXS experiments[23–25] show that such anisotropic lattice strains force the MnO_6 octahedral sites into a ferro-distortive (FD) alignment, where the FD supercell coincides with the unit cell of the crystalline lattice. Thus, it can be argued that $R_{1-x}Sr_xMnO_3$ ($x=0.4$ or 0.5) thin films with a uniaxially distorted crystal structure exhibit[23,24] a FD alignment due to epitaxial strain (extrinsic effect), whereas exactly the same stoichiometries adopt an AFD state and an orthorhombic crystal structure in their bulk form[18] because the minimization of elastic energy takes place by JT distortions (intrinsic effect).

In $[La_{2/3}Ca_{1/3}MnO_3(FM)/La_{1/3}Ca_{2/3}MnO_3(AF)]_{15}$ multilayers that exhibit EB, temperature-dependent RXS measurements at the Mn K-edge are also expected to probe the evolution of local distortions due to epitaxial strain. The relationship between pseudocubic and orthorhombic (*Pnma* space group No. 62) crystallographic directions that occur parallel and normal to film surface in $La_{2/3}Ca_{1/3}MnO_3$ FM and $La_{1/3}Ca_{2/3}MnO_3$ AF layers is detailed in Ref. 27. In $La_{2/3}Ca_{1/3}MnO_3$ thin films that grow epitaxially on $LaAlO_3(001)$, the orthorhombic c_o axis is oriented either parallel to [100] or [010] direction of the substrate (lying in the film plane) or to [001] direction perpendicular to film surface. Domains with c_o axes lying in film-plane are called $[110]_O$ oriented and those with c_o-axes normal to film surface are called $[001]_O$ oriented, because their orthorhombic $[110]_O$ and $[001]_O$ axes are perpendicular to $LaAlO_3(001)$ surface, respectively. Transmission electron microscopy (TEM) is able[27] to distinguish these two orientations. In our case, it was observed[4] that: (i) the pseudocubic [001] direction normal to film surface corresponds to $[110]_O$-type of orientation within the multilayer, and (ii) there is a considerable lattice expansion along the film normal direction. The former shows that, in *Pnma* setting, the a_o and c_o axes make an angle with the film-normal direction and the second shows that epitaxial strain should govern the local distortions in FM and AF layers. To examine the EB properties in connection with trends associated with the local distortions of $[La_{2/3}Ca_{1/3}MnO_3(FM)/La_{1/3}Ca_{2/3}MnO_3(AF)]_{15}$ multilayers, we have performed RXS measurements at the Mn K-edge.

II. EXPERIMENTAL DETAILS

$[La_{2/3}Ca_{1/3}MnO_3(3\ nm)/La_{1/3}Ca_{2/3}MnO_3(3\ nm)]_{15}$ multilayers were prepared by pulsed-laser deposition of bulk stoichiometric targets on (001)$LaAlO_3$ single-crystal substrates. The multilayers were grown on 35 nm thick $La_{0.33}Ca_{0.67}MnO_3$ (AF) buffer layer, and their FM and AF layer thicknesses were chosen to be at about the optimum exchange-biasing effect observed.[2–4] X-ray diffraction (XRD) spectra were collected at ambient conditions with a Bruker D8 diffractometer using Cu-K_α radiation. The grouping of the satellite peaks observed near the (00ℓ) Bragg-positions of the $LaAlO_3$ substrate indicates that there is a coherent AF/FM superlattice with a bilayer thickness $\Lambda = 6.1(1)$ nm (in agreement with the nominal value of 6 nm). Assuming a *pseudocubic structure* for the multilayer, the observed positions of the (001), (002), and (003) Bragg peaks provide an estimate of 3.863 Å for the *average lattice spacing* perpendicular to film surface. Similar measurements on a 45 nm thick AF (FM) film give an average lattice spacing perpendicular to film surface of 3.79 (3.95) Å. The epitaxy was revealed[4] by conventional and high resolution TEM. Dc-magnetic measurements used for magnetic characterization have shown the same magnetothermal and EB behavior as in previous studies.[3,4]

The RXS experiment has been carried out on the XMaS beam line BM28 at the ESRF in Grenoble, France.[28] The thin-film sample was mounted on the 11-axis, 6-circle Huber diffractometer within a closed-cycle He cryostat. All measurements were undertaken in triple-axis geometry near the Mn *K*-edge (on resonance) between 10 and 300 K. The incident x-ray beam was monochromated with a double-bounce Si(111) monochromator and focused using a pneumatically bent silicon mirror coated with rhodium. This gives a 96% linear and horizontal polarization of incident synchrotron radiation (96% σ-polarized) and an incident energy resolution of ~1 eV at the Mn *K*-edge. In synchrotron radiation, the strong horizontal polarization of the incident beam (referred to as σ) allows the $\sigma \rightarrow \sigma'$ and $\sigma \rightarrow \pi'$ components of the scattered beam to be detected using a polarization analyzing crystal. The σ and σ' symbols denote the unit vector $\epsilon_\sigma = \epsilon'_\sigma$ of light polarization that is *perpendicular to the diffraction plane* for the incident and diffracted beams, respectively, while π and π' are unit vectors ϵ_π, ϵ'_π *in the diffraction plane*, perpendicular to incident and diffracted beams, respectively. Linear polarization analysis of the scattered beam has been performed via rotation of a Cu(220) crystal about the scattered beam direction. For an incident photon energy set at the Mn *K*-edge, the Cu(220) scattering angle is $2\theta_A \sim 95.49°$ that results (at $E = 6.53$ keV) in 2.2% incomplete suppression of the unselected component of the scattered beam and the small π component of the incident beam, which is referred to as *leakage*.

III. RESULTS AND DISCUSSION

A. Diffraction measurements

Synchrotron x-ray diffraction measurements were performed in order to obtain information about the texture and lattice parameters of the multilayer. Figure 1 shows the diffracted intensity at 270 K for momentum transfer *L* scans along the normal direction of the film surface, where *L* denotes the continuous-valued coordinate of momentum transfer perpendicular to the surface of the sample in reciprocal lattice units (r.l.u.). Diffraction patterns for $[10L]$ and $[00L]$ scans, centered at the pseudocubic (102) and (002) Bragg peaks of the multilayer, are shown in Fig. 1(a). The most intense Bragg peak comes from the $LaAlO_3(00\ell)$ substrate. It is worth mentioning that there were no half-integer $(1,0,n/2)$ peaks detected in these *L* scans, indicating that there is no doubling of the unit cell along *L* as in $La_{2/3}Ca_{1/3}MnO_3$ epitaxial films grown on $SrTiO_3(100)$ substrates.[29] Generally, the scattered intensity $I(\mathbf{Q})$ can be decomposed into two contributions. One contribution comes from the structure factor $F(\mathbf{Q})$ and another from the *Laue function*. In XRD measurements with the wave vector transfer $Q(=L)$ perpendicular to the surface of an epitaxially grown multilayer, the *Laue function* exhibits pronounced maxima at the Bragg condition: $Q_B = 2\pi\ell/d_{av}$, where d_{av} is the lattice spacing normal to film surface. For the $LaAlO_3$ substrate the Bragg peaks at Q_B become very intense and narrow (Dirac δ function) (Fig. 2), whereas for the multilayer the Bragg peaks are broader and exhibit Laue oscillations at their tails, which are visible in Fig. 1(a) between the peaks.

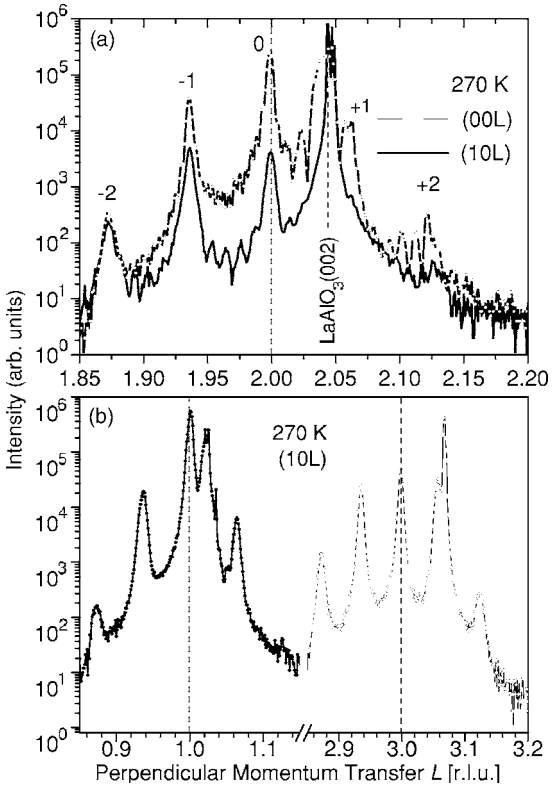

FIG. 1. Synchrotron x-ray diffraction ($\lambda = 1.4781$ Å) profiles from a $[La_{2/3}Ca_{1/3}MnO_3(3\ nm)/La_{1/3}Ca_{2/3}MnO_3(3\ nm)]_{15}$ multilayer. (a) $[00L]$ and $[10L]$ scans through the (002) and (102) pseudocubic Bragg peaks, respectively. (b) $[10L]$ scans through the (101) and (103) Bragg peaks. The peak labels indicate the order number ($n = 0, \pm 1, \pm 2$) of the satellite reflections from the multilayer structure.

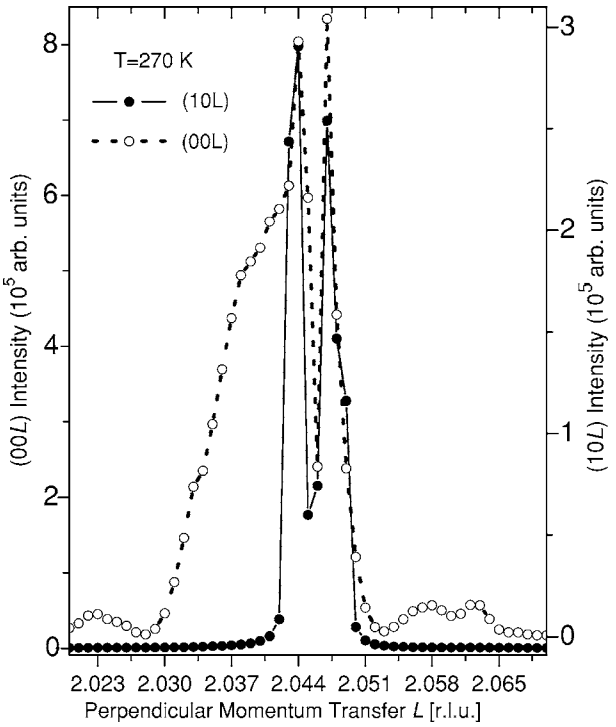

FIG. 2. Expanded view of the diffraction profile of Fig. 1(a), focusing on the (002) and (102) Bragg peaks of the $LaAlO_3$ substrate in the $[00L]$ and $[10L]$ scans.

In Fig. 1(a), the number of Laue oscillations between two consecutive superlattice reflections equals the number of atomic layers N in the AF/FM bilayer. Fifteen Laue oscillations (13+2 hidden under the two peaks) can be resolved in between the zeroth order and the $n=-1$ superlattice peaks for the $[00L]$ scan [Fig. 1(a)]. A bilayer thickness of 5.8 nm is obtained by multiplying $N=15$ with the average lattice parameter, $d_{av}=0.3863$ nm of the pseudocubic unit cell. Alternatively, the spacing between subsequent superlattice peak positions, $\Delta L=1/N$, gives a bilayer thickness of $\Lambda=6.07(1)$ nm when $N=1/\Delta L$ is multiplied by the average lattice parameter $d_{av}=0.3863$ nm. The difference of 0.27 nm in Λ between the two calculations is due to the fact that there is no integer number N of atomic layers in each bilayer, and thus, the number of Laue oscillations is between 15 and 16. In our case, a noninteger number N of atomic layers in each bilayer arises from roughness and strain effects at the AF/FM interfaces, which determine the envelope of the intensity of Laue oscillations. Figure 1(a) shows that, along the $[00L]$ scan, the intensities of Laue oscillations are attenuated before the zeroth-order (002) peak of the multilayer, whereas for larger L their intensities become comparable to superlattice reflections, creating the wrong impression that the satellites with $n=+1$ and $n=+2$ are split. Such an asymmetric intensity of the satellite peaks[30] and of Laue oscillations[31] has been reported in multilayers that exhibit chemical and/or strained interfacial profiles along the growth direction. This asymmetry of peak intensities among the positively and negatively signed satellites is removed when similar multilayers that exhibit a relatively moderate EB effect are grown[32] on lattice matched substrates. This is an unambiguous evidence for the predominant role of epitaxial strain, which is induced by the lattice mismatched $LaAlO_3$ substrate on the anisotropy of lattice distortions within the multilayer structure.

Figure 1(b) shows the distribution of intensity at 270 K around the (101) and (103) pseudocubic Bragg peaks. The observed pattern of Bragg peaks and superstructure reflections does not change down to 10 K. However, Laue oscillations are hardly visible in the $[10L]$ scans (Fig. 1) because of the orientation of the crystallographic planes relative to the normal direction to the film. The $[10\ell]$ crystallographic directions are not parallel to the normal, as in the $[00\ell]$ case. Since $(La,Ca)MnO_3$ thin films exhibit extensive twinning when they adopt the *Pnma* structure,[27] Fig. 2 shows an expanded version of Fig. 1(a) focusing on the Bragg-peak splitting of the $LaAlO_3$ substrate (which is related to crystal twinning). Two main features can be observed for the $(00L)$ and $(10L)$ scans:

(i) Peak splitting into two very sharp peaks located at $L=2.044$ and 2.047 r.l.u. occurs for both $[00L]$ and $[10L]$ scans with $L=1,2,3$. The full width at half maximum (FWHM) of these peaks is less than 0.001 r.l.u. Such extremely narrow peaks are reminiscent of XRD θ-rocking curve peaks observed[33] in $LaAlO_3(001)$ single crystal substrates due to twinning. The (002) Bragg peak from the multilayer in Fig. 1 and the θ-rocking curve peak from the sputter-grown $La_{2/3}Ca_{1/3}MnO_3$ FM thin film in Ref. 33 show no such splitting. The reason might be that, in both cases, the corresponding twin angle[33] is too small to grow separately on each twin plane.

(ii) Only $[00L]$ scans exhibit a broad peak shoulder with strong intensity located at ~2.04 r.l.u. and with a FWHM of $\Delta L_{buf}=0.0112$ r.l.u. This corresponds to a number of atomic layers $N_{buf}=89$, which when multiplied by 0.38 nm (the observed d-spacing of a 45 nm thick AF thin film) leads to a 33.8 nm buffer layer thickness (comparable to the nominal thickness of 35 nm). Thus, the broad peak can be assigned to the AF buffer layer. Its presence along the $[00L]$ scan is due to a slight lattice mismatch with the $LaAlO_3(001)$ single crystal that exhibits a d_{av}-spacing of 0.379 nm on a free-standing substrate.

In order to determine the temperature dependence of the pseudocubic a and c lattice parameters, θ-2θ scans were performed on the (101) and (102) Bragg reflections. Since any arbitrary reflection $(hk\ell)_c$ in the pseudocubic subcell is transformed to the *Pnma* unit cell as: $(h,k,\ell)_c=(h+\ell,2k,h-\ell)_O$, these two reflections can be indexed as: $(101)\rightarrow(200)_O$ and $(102)\rightarrow(30\bar{1})_O$. Pseudocubic lattice parameters assuming *Pnma* are: $a^2=(a_o/2)^2+(c_o/2)^2$ and $c=b_o/2$. Figure 3 shows the temperature dependence of the pseudocubic $d_{h0\ell}$-spacings and the corresponding FWHM, extracted by fitting the observed Bragg peaks with a Lorentzian squared line shape. The pseudocubic lattice parameters $a=a_{ML}$ and $c=c_{ML}$ and the in-plane $\epsilon_{100}=(a_{bulk}-a_{ML})/a_{bulk}$ and out-of-plane $\epsilon_{001}=(c_{bulk}-c_{ML})/c_{bulk}$ lattice strain values are plotted as a function of temperature in Fig. 4 together with the observed[5] AF-c_{bulk}, AF-a_{bulk}, and[34] FM-c_{bulk}, FM-a_{bulk} bulk parameters $[a^2_{bulk}=(a_o/2)^2+(c_o/2)^2$ and c_{bulk}

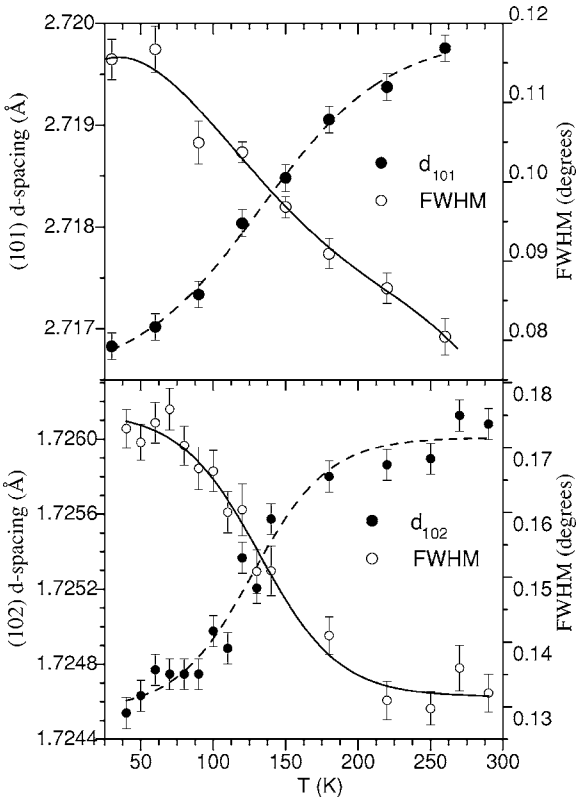

FIG. 3. Temperature dependence of the *d*-spacing and FWHM for the (101) and (102) pseudocubic Bragg reflections of the multilayer, measured on resonance. Lines are guides to the eye.

$=b_o/2]$ that correspond to the stoichiometry of the AF buffer and AF, FM layers in the multilayer structure. The calculated in-plane $\epsilon_{100}=\epsilon_{010}$ and out-of-plane ϵ_{001} lattice strains are based on the assumption of pseudocubic (001) growth on the AF buffer, providing an estimate for the deviation of $a=a_{ML}$ and $c=c_{ML}$ parameters from those of the AF bulk (AF buffer) as a function of temperature.

Figure 5 displays the pseudo-cubic $a=a_{ML}$ (○), $c=c_{ML}$ (□) lattice parameters between 30 and 260 K (left-hand axis) together with the calculated (right-hand axis) strain difference $\delta\epsilon=\epsilon_{001}-\epsilon_{100}$ (▲), that follows the temperature dependence of the lattice parameter a below the T_C(~250 K). The top panel shows the temperature dependence of the axial ratio c/a and of the $\delta\epsilon(T)/\delta\epsilon$(260 K) ratio. The c/a ratio is always >1, indicating laterally (in-plane) compressive strain. The inset (Fig. 5) shows tentatively assigned ratios of Young moduli, $Y_{\mathrm{FM}}/Y_{\mathrm{AF}}$, as a function of temperature. Figures 4 and 5 reveal a major change of lattice parameters around the observed T_C(≈250 K) and a relatively moderate change around the observed T_B (≈80 K) of the multilayer. Note that both pseudocubic lattice parameters (Fig. 4) converge above the T_C(=250 K) of the multilayer, following the trend of the AF bulk above its CO transition T_{CO}(≈240 K). Assuming elastically strained multilayers, the common lattice parameter $\bar{a}$ at the AF/FM interfaces can be estimated[35] from the bulk Young moduli Y_{AF}, Y_{FM} and bulk lattice parameters of the individual layers. If the strain forces are equilibrated at the AF/FM interfaces, then[35]

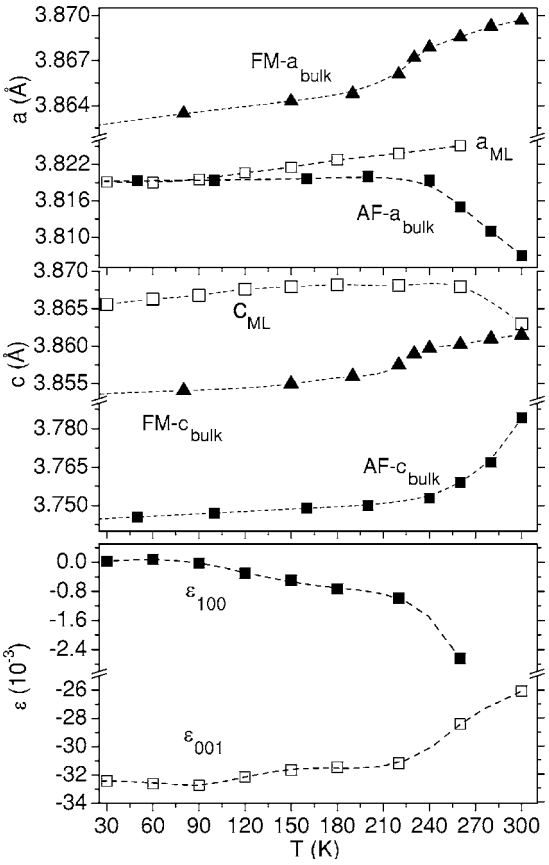

FIG. 4. Temperature dependence of the lattice parameters c_{ML}, AF-c_{bulk}, FM-c_{bulk} and a_{ML}, AF-a_{bulk}, FM-a_{bulk} where the bulk parameters correspond to the stoichiometry of the AF buffer and of the AF, FM layers in the multilayer. The bottom panel shows the in-plane $\epsilon_{100}=(a_{\mathrm{bulk}}-a_{ML})/a_{\mathrm{bulk}}$ and out-of-plane $\epsilon_{001}=(c_{\mathrm{bulk}}-c_{ML})/c_{\mathrm{bulk}}$ lattice strain values with respect to the bulk AF component. Lines are guides to the eye.

$$\bar{a}=a_{\mathrm{FM}}a_{\mathrm{AF}}\left(\frac{1+\frac{Y_{\mathrm{FM}}t_{\mathrm{FM}}}{Y_{\mathrm{AF}}t_{\mathrm{AF}}}}{a_{\mathrm{FM}}+\frac{Y_{\mathrm{FM}}t_{\mathrm{FM}}a_{\mathrm{AF}}}{Y_{\mathrm{AF}}t_{\mathrm{AF}}}}\right). \quad (1)$$

For equal AF and FM layer thicknesses, $t_{\mathrm{AF}}=t_{\mathrm{FM}}=3$ nm, unstrained (bulk) pseudocubic lattice parameters $a_{\mathrm{FM}}=3.869$ Å, $a_{\mathrm{AF}}=3.80$ Å at 300 K, and assuming that $Y_{\mathrm{AF}}\approx Y_{\mathrm{FM}}$ we obtain an $\bar{a}=3.834$ Å. Given the arbitrary approximation: $Y_{\mathrm{AF}}=Y_{\mathrm{FM}}$, a deviation of $\bar{a}$ by 0.009 Å from the observed $a_{ML}=3.825$ Å at 260 K (Fig. 4) indicates that a_{ML} is the result of elastically deformed bulk lattice parameters above the observed $T_C=250$ K. In this approximation, the pseudocubic parameters from Fig. 4 can be used as the known parameters in Eq. (1) to obtain some indicative $Y_{\mathrm{FM}}/Y_{\mathrm{AF}}$ film-ratios above and below the T_C,

$$\frac{Y_{\mathrm{FM}}}{Y_{\mathrm{AF}}}=\frac{a_{\mathrm{FM}}(a_{\mathrm{AF}}-\bar{a})}{a_{\mathrm{AF}}(\bar{a}-a_{\mathrm{FM}})}, \quad (2)$$

where $t_{\mathrm{AF}}=t_{\mathrm{FM}}=3$ nm in Eq. (1). Substitution of the bulk lattice parameters a_{FM}, a_{AF}, and $a_{ML}=\bar{a}(T)$ from Fig. 4 in Eq.

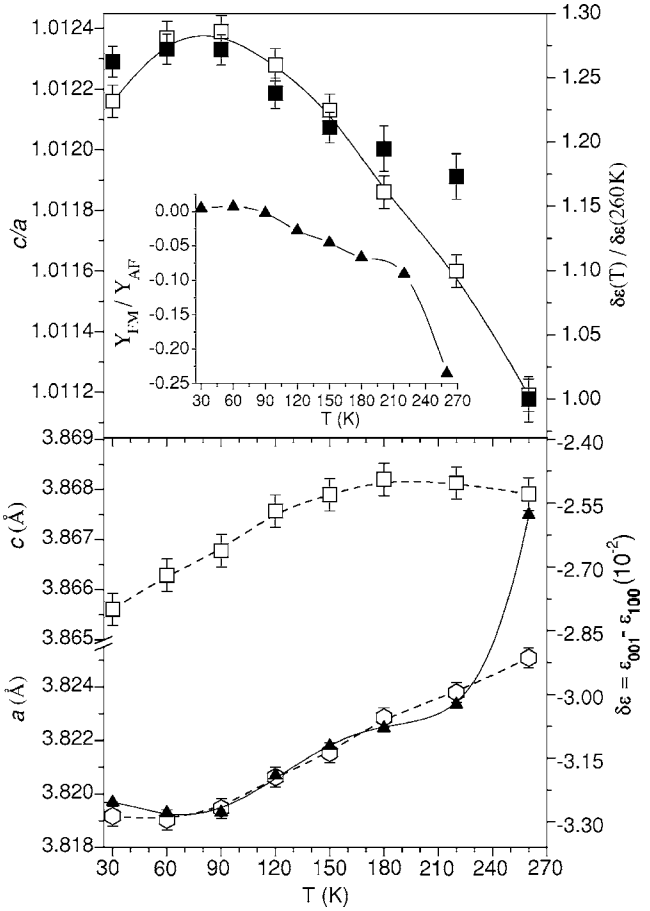

FIG. 5. Top panel: Temperature dependence of axial (□) c/a (left-hand axis) and strain-difference (■) $\delta\epsilon(T)/\delta\epsilon(260\ \mathrm{K})$ (right-hand axis) ratios. The inset shows the $Y_{\mathrm{FM}}/Y_{\mathrm{AF}}$ ratios (▲), calculated from Eq. (2) between 30 and 260 K. Bottom panel: Temperature dependence of the pseudocubic lattice parameters a (○), c (□) between 30 and 260 K (left-hand axis) and of the strain difference (▲) $\epsilon_{001}-\epsilon_{100}$ (right-hand axis). Lines are guides to the eye.

(2) allows the calculation of the $Y_{\mathrm{FM}}/Y_{\mathrm{AF}}$ ratio as a function of temperature. The inset of Fig. 5 shows the results, revealing that below 90 K the resistance of the FM layers to elastic deformation (stiffness) becomes zero because a_{AF}-$\bar{a}$ is practically zero (10^{-4} Å). It means that accommodation of strains at the FM/AF interfaces cannot take place only by elastic deformation of the corresponding FM and AF bulk lattice parameters at lower temperatures. This is a first evidence that strain-driven lattice deformations induce disorder, which may pin the local distortions below the T_B. Recent studies[36,37] have shown that epitaxial (biaxial) strain affects the JT distortions and reduces the transition temperature (T_C or T_p) in CMR multilayers. The present study investigates the temperature dependence of epitaxial strain in AF/FM CMR multilayers that exhibit a $T_B \approx 80$ K well below the observed $T_C=250$ K.

A comparison between the pseudocubic lattice parameters obtained for the bulk form of the AF layer (conversion from Fig. 2 in Ref. 5 to pseudocubic parameters) and those in Fig. 4, indicates that, first, the in-plane lattice parameter of the multilayer (a-axis) contracts, whereas in the bulk[5] it expands on cooling, and second, at ~90 K it approaches the value of $a=3.819$ Å, which is comparable to that in the AF bulk. Considering the thermal expansion coefficient $\eta_s \approx 1.1 \times 10^{-5}\ \mathrm{K}^{-1}$ of $LaAlO_3$, the magnitude of the thermal tensile strain exercised in the film-plane between 30 and 260 K is: $\epsilon_{100}(T)=\eta_s \Delta T=0.00253$, which added to $a_{ML}(T=30$ or 90 K$)=3.819$ Å gives an $a_{ML}(260\ \mathrm{K})=3.821$ Å (observed 3.825 Å). However, both $\epsilon_{001}(T)$ and $\epsilon_{100}(T)$ functions do not follow a linear thermal expansion between 30 and 260 K. This behavior shows that compressive strains exercised by the thermal contraction of the $LaAlO_3$ substrate on cooling are counterbalanced between the [substrate/AF-buffer] and [AF-buffer/multilayer] interfaces up to the elastic limit of the multilayer. This limit is reached when the pseudocubic lattice constant-a of the multilayer approaches the bulk value $a_{\mathrm{bulk}}=3.819$ Å, of the AF layers below the T_B. Electron microscopy (TEM) measurements have shown[4] that the AF-buffer layer is coherently strained by the $LaAlO_3$ substrate (there is no detectable difference between the in-plane d-spacing of the $(0h0)$ planes between the $LaAlO_3$ and AF-buffer structures) at ambient conditions. Thus, the observed deviation of $a_{ML}(T)$ and $c_{ML}(T)$ parameters from a linear thermal expansion at ~90 K (Fig. 5) can be attributed to strain-driven disordering that may pin local distortions in the AF and FM layers as a_{ML} approaches the AF-a_{bulk}.

It was observed[38] that the magnetic anisotropy of epitaxial $La_{0.7}Sr_{0.3}MnO_3$ thin films is dominated by the strain or magnetocrystalline anisotropy, depending on the orientation of the film. Accordingly, the obtained ϵ_{001} and ϵ_{100} values in Figs. 4 and 5 can be associated with the magnetoelastic (ME) coupling inside the AF and FM layers. Considering only elastic deformations, the ME energy density is: $f_{\mathrm{me}}^{\mathrm{cubic}}=B_1^{\mathrm{eff}}\epsilon_{100}(T)$, and the intrinsic stress of a pseudocubic (001)-film can be formulated[39] as a magnetostrictive stress: $\tau_{\mathrm{me}}=\partial f_{\mathrm{me}}/\partial\epsilon_{100}$. In the simplest form,[39] B_1^{eff} is equal to the first-order ME coupling coefficient B_1, and the $\tau_{\mathrm{me}}=B_1(T)$ is constant at a given temperature no matter how large the initial strain is. It has been argued[40] that the volume contribution to the magnetic anisotropy energy (K_V) in tetragonal distorted (fct) Ni films, is proportional to c/a ratio for constant volume distortions. The dependence of K_V on c/a has been ascribed[40] to the ME coupling: $K_V=(3/2)\lambda_{100}(c_{11}-c_{12})(\epsilon_\perp-\epsilon_\parallel)$. Since[39] the magnetostriction constant: $\lambda_{100}=-(2/3)B_1(c_{11}-c_{12})^{-1}$ then $K_V=-B_1(\epsilon_\perp-\epsilon_\parallel)$. In our case, $\delta\epsilon=\epsilon_\perp-\epsilon_\parallel=\epsilon_{001}-\epsilon_{100}$ whereas the volume of the pseudocubic unit cell changes only slightly, between 56.6 Å^3 at 260 K and 56.4 Å^3 at 30 K. The top panel of Fig. 5 shows that the $\delta\epsilon(T)/\delta\epsilon(260\ \mathrm{K})$ ratio follows the temperature dependence of the c/a ratio for nearly constant volume distortions between 30 and 260 K, suggesting that K_V relates with the c/a ratio via the ME coupling as in fct Ni films.[40] Considering that $K_V(T)/K_V(260\ \mathrm{K})=[B_1(T)/B_1(260\ \mathrm{K})][\delta\epsilon(T)/\delta\epsilon(260\ \mathrm{K})]$, it can be inferred that both K_V and c/a saturate at lower temperatures because the strain difference $\delta\epsilon$ reaches its absolute maximum below 90 K (bottom panel in Fig. 5). Since the ME coupling (strain) may even determine[38] the magnetic anisotropy of CMR films, the temperature dependence of strain ratios in Fig. 5 shows that strain-driven effects are related with the EB effect via the ME coupling.

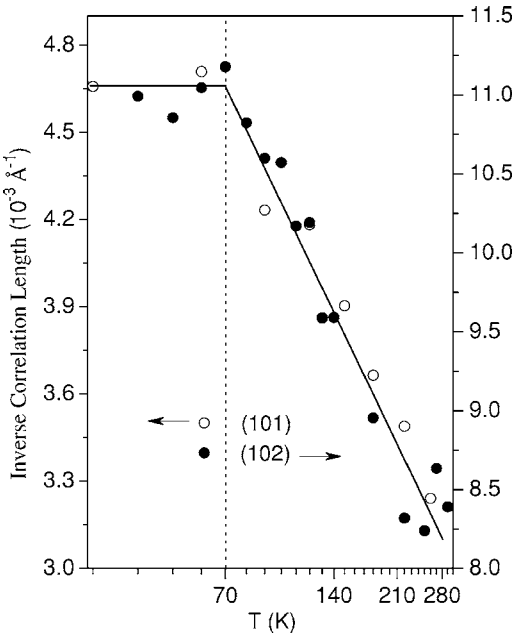

FIG. 6. Temperature dependence of the inverse correlation length ξ^{-1}, obtained from θ-2θ scans of the pseudocubic (101) and (102) Bragg peaks. The grid line at 70 K marks the temperature range below which EB is observed. Lines are guides to the eye.

The relatively large increase of the c/a ratio observed on cooling (Fig. 5) is mainly due to the epitaxial lattice contraction of a, since $(\Delta a/a) \approx 0.14\%$ and $(\Delta c/c) \approx 0.06\%$ between 260 and 30 K. Most importantly, both the c/a and $\delta\epsilon(T)/\delta\epsilon(260\ \mathrm{K})$ ratios become maximum at the same temperature where the EB effect is observed[3] ($T_B \approx 80$ K). The most marked changes occur in $\delta\epsilon(T)$, where a change of 10% is obtained (Fig. 5) between 260 and 60 K at the T_B, indicating that: (i) EB sets in when there is an additional strain difference ($\sim 10\%$) between a-axis and c-axis directions below the T_C, and (ii) both $\delta\epsilon(T)$ and $K_V(T)$ saturate at the T_B because $a_{ML} \approx a_{\mathrm{bulk}}$ of the AF layer in its bulk form.

Figure 6 shows the temperature dependence of the inverse correlation length, ξ^{-1} calculated by the expression: $\xi^{-1} = \pi(\mathrm{FWHM})/d_{h0\ell}$, using values of the FWHM and of d_{101}-, d_{102}-spacings from Fig. 3. Similar temperature dependence of ξ^{-1} is found for both Bragg reflections. In Fig. 6, ξ^{-1} remains constant up to about 70 K and then it decreases progressively at higher temperatures, following the temperature dependence of the axial c/a and strain difference $\delta\epsilon(T)/\delta\epsilon(260\ \mathrm{K})$ ratios (Fig. 5). This resemblance suggests that ξ is related to the coherent modulation length of local distortions that are commensurate with the crystallographic unit cell of the multilayer. Notably, the slope change observed in the thermal response of ξ at ~ 70 K occurs at the same temperature below which EB is observed.[2–4] For the pseudocubic (101) Bragg-peak, the correlation length ξ_{101} decreases from 30 nm at 250 K to 21 nm below the T_B (note that ξ_{102} is about half of ξ_{101}). Such small correlation lengths (relative to bulk samples) can be associated with the increase of strain in the FM layers as a_{ML} approaches the a_{bulk} value of the AF bulk layer at lower temperatures (Fig. 5). Thus, $\xi^{-1}(\xi)$ reaches its maximum (minimum) value when $a_{ML} \approx \mathrm{AF}-a_{\mathrm{bulk}}$ because the FM layers are strained to maximum levels (by comparing the lattice parameters in Fig. 4). However, equilibration of strains at the AF/FM interfaces may introduce disorder in FD octahedral tilt ordering. This disorder may pin the local distortions below 300 K and, thus, the coherent modulation length of local lattice distortions decreases progressively down to 70 K following the accommodation of strain inside the AF and FM layers.

The above results show that the axial ratio c/a, the strain difference $\delta\epsilon(T)/\delta\epsilon(260\ \mathrm{K})$ ratio, and the correlation lengths follow the temperature dependence of a_{ML}. It shows that epitaxial strain competes the electron-lattice coupling[26] due to JT distortions and participates predominantly in creation of local distortions below the T_C. The effect of epitaxial strain on local distortions is examined in the next section as a function of temperature.

B. RXS experiment

All RXS measurements were performed on warming from 10 to 300 K without applying an external magnetic field. First, we searched for the existence of resonant (forbidden) reflections from the AFD supercell[5] in the multilayer and in a 45 nm thick $La_{1/3}Ca_{2/3}MnO_3$ AF film without any success. The fact that we could not detect the AFD reflections even in the AF thin film shows clearly the dominance of epitaxial strain on lattice distortions. In a previous study,[41] it was reported that very weak AFD reflections were observed in a 150 nm thick $La_{1/3}Ca_{2/3}MnO_3$ (AF) film grown on $SrTiO_3$, by H-, K-, and L-scans through the $\left(\frac{4}{3},2,1\right)_O$ and $\left(\frac{2}{3},2,1\right)_O$ resonant peaks. Since $SrTiO_3$ is not a good choice of substrate for lattice-matching growth of AF $La_{1/3}Ca_{2/3}MnO_3$ films and the film thickness was about three times larger than that of our AF film, these measurements[41] came from a strain-relaxed (bulklike) AF film where the lattice mismatching with the substrate has precluded epitaxial growth (probably both orthorhombic $[110]_O$ and $[001]_O$ orientations[27] existed in the film).

Some differences between the structures of the AF thin film and the AF/FM multilayer are demonstrated in Fig. 7, where exploratory fluorescence measurements at 10 K are shown for both films examined in the present study. The x-ray absorption near-edge structure (XANES) data from the 45 nm thick AF film exhibit three pre-edge peaks, which have been assigned according to Ref. 42 and are not discussed here. A number of differences between the main absorption edges of the multilayers and the AF thin film can be resolved. First of all, the multilayer exhibits a positive energy shift of $\sim 1.5(5)$ eV in the position of the main-edge jump relative to that in the AF-film because, given the FM-a_{bulk} values in Fig. 4, the FM layers are subjected to a more compressive[43] strain in the multilayer structure than the lattice-matched AF film grown onto $LaAlO_3$ substrate. In addition, a shoulder at the basis of the main edge provides evidence for a double edge structure in the AF film, indicating[44] two distinct Mn valence states. Another evidence[44] for two completely localized Mn^{3+} and Mn^{4+} ions in the AF film is the smaller average slope of the main-edge peak in Fig. 7. In addition, the intense XANES peak just

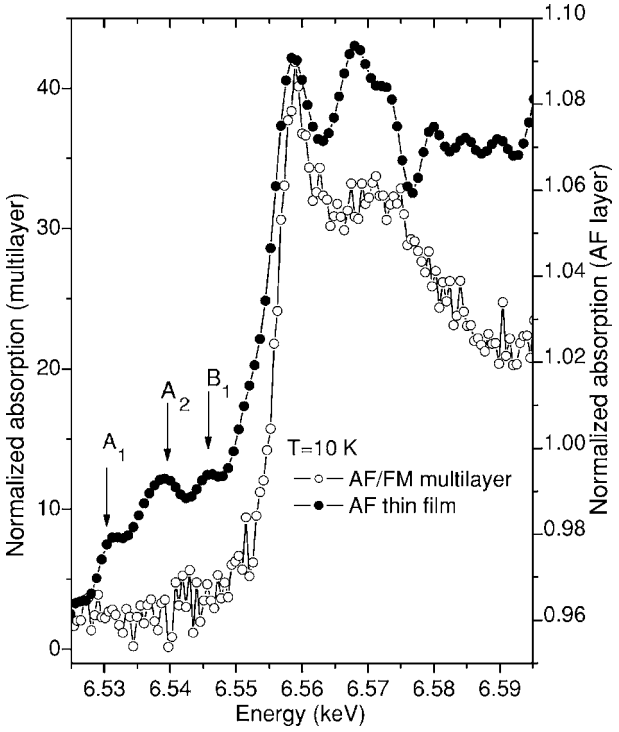

FIG. 7. Comparison between the XANES fluorescence spectra of the multilayer and a 45 nm thick AF film grown on $LaAlO_3(001)$ substrate. Pre-edge peaks have been assigned according to Ref. 42.

before the 6.57 keV feature, which is observed only in the AF film, can be assigned to a second main-edge absorption peak arising from a Mn(4+) valence state. Thus, we may consider that there is a double-peak absorption edge (two main edges) in the AF film due to two completely localized Mn(3+) and Mn(4+) valence states in the CO phase at 10 K. However, the analysis of these two features is far beyond the scope of the present study since we focus here in the study of the multilayer. In the postedge region the multilayer exhibits bulklike[44,45] XANES and the postedge peak at ~6.57 keV is very broad, indicating a mixing of Mn^{3+} and Mn^{4+} valence states which can be described[46] either as fluctuating charges between different ionic sites due to electron hopping or as a system formed by a core of Mn^{4+} ions where itinerant electrons move around among the different ions. The intensity and shape of this postedge resonance depends strongly on the scattering of the outgoing photoelectron by coordination shells beyond the first shell of the MnO_6 octahedron, and its temperature dependence is discussed below.

Previous RXS experiments[23–25] on different thin films that exhibit a FD alignment have examined the RXS signals of the (102) Bragg reflection. In the present experiment, systematic RXS measurements were also performed at the pseudocubic (102) reflection. In the geometrical arrangement adopted for the RXS experiment, we consider an incident x-ray with energy $\hbar\omega$, wave vector k and horizontal polarization ϵ (σ-polarized) that undergoes the dipolar transition process inside the sample. At the Bragg angle θ, the scattered x-ray has the same energy (elastic scattering), wave vector k', and polarization ϵ' with σ' and π' components. In order to obtain information about the anisotropic tensor of susceptibility (ATS) signal from the multilayer, RXS measurements were performed for the $\sigma \rightarrow \pi'$ channel. A Cu(220) polarization analyzer was used to pick up the ATS signal from the diffracted beam on the (102) Bragg reflection. It is worth emphasizing that, in the bulk form of the manganites,[6,17,21] dipolar RXS experiments measure directly the ATS signal by placing the detector at $\phi_A=90°$ and detecting only the π'-polarized scattered beam at a resonant reflection from the AFD supercell (ϕ_A is the rotation angle of the detector around the scattered wave vector k' from the sample, with $\phi_A=0°$ for the $\sigma \rightarrow \sigma'$ channel and $\phi_A=90°$ for the $\sigma \rightarrow \pi'$ channel). However, in the present case, the diffraction spots from the FD alignment, which is induced by tetragonal lattice distortions, coincide with Bragg-reflections and, thus, contamination of the signal from the stronger $[(\sigma \rightarrow \sigma')_B]$ Bragg scattering overpowers the very weak signal from the $\sigma \rightarrow \pi'$ component that we look for. The interference technique[23–25] can counterbalance this contamination by the subtraction,

$$I(90° + \delta\phi_A) - I(90° - \delta\phi_A) \propto 2Re[F_{\sigma\sigma'}F^*_{\sigma\pi'}]\sin^2 2\theta_A \sin 2\delta\phi_A, \quad (3)$$

where $F_{\sigma\sigma'}$ and $F_{\sigma\pi'}$ are the FD structure factors for the $(hk\ell)$ fundamental Bragg-reflection, which are applicable for $\sigma \rightarrow \sigma'$ and $\sigma \rightarrow \pi'$ reflections, respectively, $2\theta_A$ is the angle by which the analyzer should deflect the scattered beam from the sample perpendicular to the wave vector k', and $\delta\phi_A$ is the angular deviation from $\phi_A=90°$ in $\sigma \rightarrow \pi'$ channel, However, preliminary momentum transfer scans along the H principal direction in reciprocal space have shown forbidden[47,48] (Templeton) reflections at (0.5,0,1), (1.5,0,1), (0.5,0,2), and (1.5,0,2) for the $\sigma \rightarrow \sigma'$ channel, which cannot be taken into account for the calculation of the FD structure factors with the available data. Such reflections, with half-integer pseudocubic indices, have been treated[29] as different atomic displacements from a metrically tetragonal perovskite to obtain the extra peaks observed in diffraction patterns along L-scans. However, in our case, these half-integer pseudocubic index reflections were observed only along H-scans and cannot be reproduced by the displacement of the La-ion from its crystallographic position in *Pnma* or *Pbnm* settings, as in Ref. 29. Additional RXS experiments are planned to provide complementary information for the estimation of the required structure factor that takes into account these extra peaks along H-scans.

For comparison to similar experiments,[23–25] RXS interference measurements were performed on the pseudocubic (102) Bragg reflection with a deviation $\delta\phi_A=\pm30°$ from the $\sigma \rightarrow \pi'$ channel configuration. Figure 8 shows the temperature dependence of the RXS profiles with the intensities, $I(\phi_A=60°)$ and $I(\phi_A=120°)$ normalized to monitor counts and to the intensity of each spectrum at 6.5575 keV (white line). These are reminiscent to those observed in Ref. 23. The intensity difference $I(\phi_A=120°)-I(\phi_A=60°)$ is plotted in Fig. 9 after subtracting a base line from the spectrum that corrects for the background contribution outside the Mn K-edge region. For comparison, the observed XANES

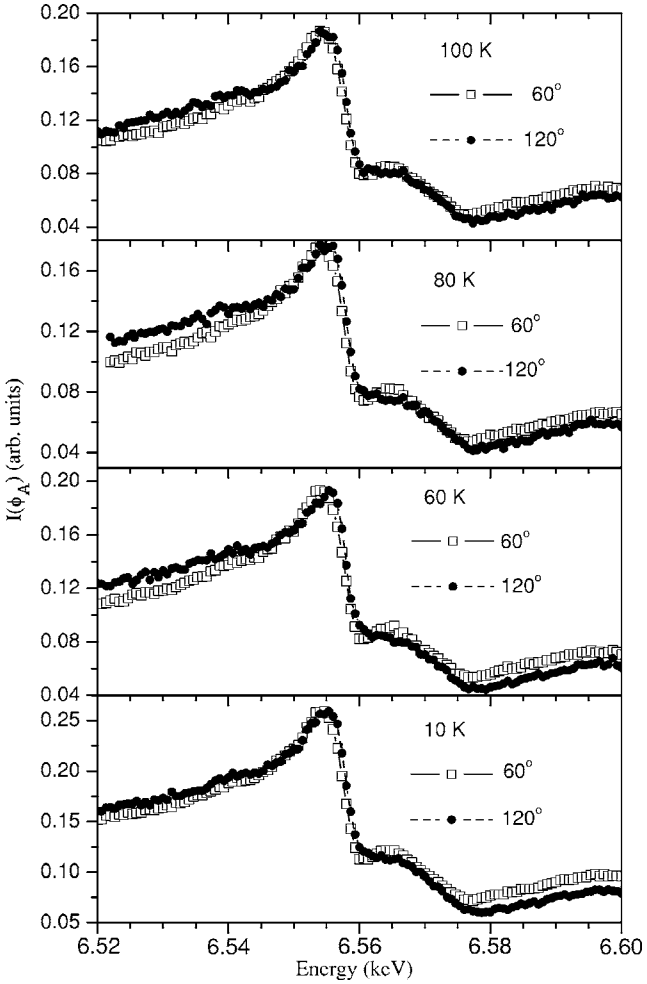

FIG. 8. RXS profiles of the pseudocubic (102) Bragg reflection. Intensities $I(\phi_A=120°)$ and $I(\phi_A=60°)$ were obtained at the same azimuthal angle and were normalized to monitor counts.

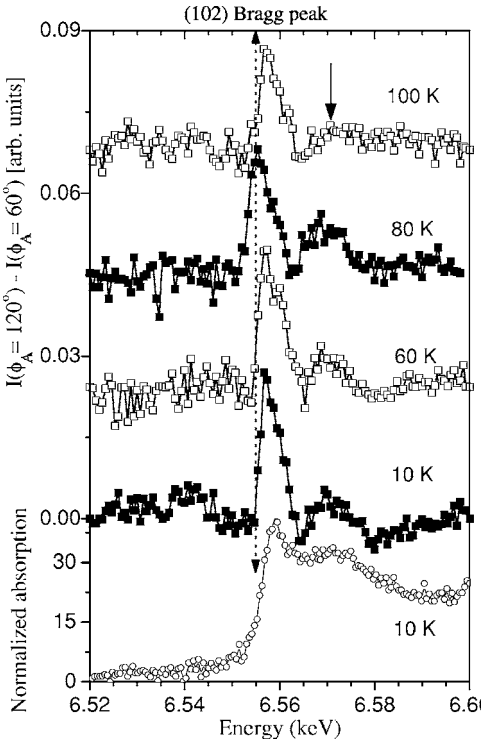

FIG. 9. Energy dependence of the difference term: $I(\phi_A=120°)-I(\phi_A=60°)$, on the pseudocubic (102) Bragg reflection, containing the contribution of $\mathrm{Re}[F_{\sigma\sigma'}F^{*}_{\sigma\pi'}]$, from the $\sigma\rightarrow\pi'$ component. The dotted line marks the energy of the white line and the arrow shows the disappearance of the intensity feature at 100 K. For comparison, the XANES spectrum of the multilayer is given at the bottom.

spectrum of the multilayer is plotted in Fig. 9. Comparing the intensity difference RXS spectra with the corresponding XANES spectrum, it becomes evident that the most intense RXS feature can be assigned to the main Mn *K*-edge and the weaker feature to the post-edge resonance. Unfortunately, due to sample positioning in the cryostat we could not perform azimuthal scans with the available triple axis geometry. However, the line shapes in Fig. 9 are almost identical with the interference signal observed[23] in $La_{0.5}Sr_{0.5}MnO_3$ epitaxial films grown on $LaAlO_3$ substrates (with $c/a>1$ as well), evidencing a similar physical origin in both interference signals that is due to FD alignment. The energy line shapes in Fig. 9 exhibit two distinct resonant features with energy positions at the Mn *K*-edge and at ~6.57 keV, respectively. Least-squares fitting of both features with Gaussian line shapes gave a linearly decreasing energy shift of the post-edge peak up to 80 K, whereas the energy shift of the main-edge peak fluctuates. The implications of these results on local distortions of the multilayer structure are discussed below.

Appropriate analysis[24] of the difference spectra $I(90°+\phi_A)-I(90°-\phi_A)$ from epitaxial films of *homogeneously* doped manganites revealed a linear energy shift of the main-edge peak as a function of the tetragonal distortion of the MnO_6 coordination polyhedron. This distortion can be induced in epitaxial films either by changing the ionic radius of the lanthanide in the doped manganite[24] or by exercising different epitaxial strains[23] in thin films of fixed stoichiometry, which are grown on substrates with different lattice matching at the interface. In strained films of CMR manganites, similar tetragonal distortions of the MnO_6 coordination polyhedron induce similar energy shifts in[43] XANES and[23] RXS spectra, indicating that both kinds of measurements probe the energy shift of the Mn *K*-edge position due to epitaxial strain. However, in our case, the width of the pair distribution function (PDF), $\sigma_{\mathrm{PDF}}=\sqrt{\frac{1}{3}\Sigma_i[(Mn-O)_i-\langle Mn-O\rangle]^2}$, may exhibit a zero shift because it averages over the local distortion of Mn-O bonds inside AF and FM layers with competing tensile and compressive strains. Thus, the obtained fluctuation of energy shift at the main-edge feature (Fig. 9) may signify that the net (averaged overall) distortion of the MnO_6 coordination polyhedron appears to be unchanged due to *compositional modulation* in the multilayer structure.

Thus, instead of the main-edge peak, it is the energy position of the postedge feature that varies linearly with both, the temperature and the reduced $(c/a)-1$ ratio below 80 K (Fig. 10). Analysis of Mn *K*-edge XANES spectra has shown that the intensity of the corresponding postedge peak de-

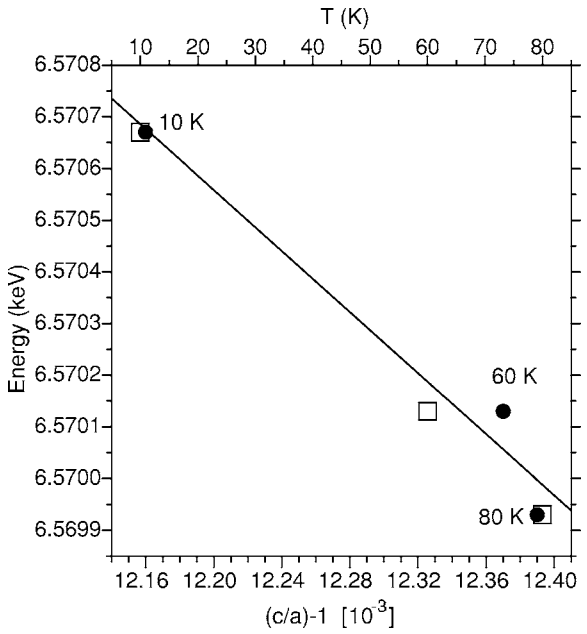

FIG. 10. Energy of the broader resonant feature observed in Fig. 9, as a function of the reduced axial ratio $(c/a)-1$ (dark symbols) and temperature (open symbols). The solid line is a linear fit of energy position versus $(c/a)-1$.

pends on contributions[49] from the eight (La,Ca)-sites surrounding a MnO_6 octahedron. Mn *K*-edge Fourier transformed *r*-space EXAFS data[50] indicate that Mn-La (Mn-Ca) pair distances are ~3 Å. In addition, x-ray circular magnetic dichroism (XCMD) spectra, observed[46] from a $La_{2/3}Ca_{1/3}MnO_3$ sample at 50 K, exhibit a strong feature 16 eV above the Mn *K*-edge. This XCMD intensity is located at ~6.57 keV as well, and comes[46] from the first shell of magnetic Mn nearest-neighbors surrounding a MnO_6 octahedron (note that Mn-O-Mn bonding angles determine the nature of magnetic coupling in doped-manganites). These results show that the intensity and the peak shape of the postedge resonance is sensitive to the radial distribution of (La,Ca)- and first nearest-neighbor Mn sites [see Figs. 1 and 2(a) in Ref. 46]. Thus, the linear decrease of the postedge energy position (Fig. 10) probes the local distortion of Mn-O-Mn bonding angles (if σ_{PDF} remains unchanged) and/or Mn-La (Mn-Ca) pair distances as a function of temperature.

The disappearance of this feature (Fig. 9) ~80 K in coincidence with: (i) the decrease in the c/a axial ratio (Fig. 5), (ii) the decrease in the inverse correlation length (Fig. 6), and (iii) the T_B, may signify a rearrangement of Mn-O-Mn bonding angles because equilibration of strains at the AF/FM interfaces induces disorder in FD octahedral tilt ordering. This disorder must pin the local distortions, which would also suppress the hopping frequency of charge carriers. In agreement, the resistivity of this multilayer increases[3] progressively by four orders of magnitude down to 80 K($=T_B$), evidencing a drastic reduction of electron hopping among the Mn sites. As the hopping frequency of the charge carriers slows down below the T_B any processes with fluctuation times larger than the interaction time[46] ($\sim 10^{-19}$ s) of the photoelectric process can be detected as local distortions. Thus, a nonzero intensity difference $I(\phi_A=120°)-I(\phi_A=60°)$ at 6.57 keV (Fig. 9) can be attributed to anisotropic[51] x-ray absorption spectra (XAS) that might be able to discriminate between two atoms of the same species at different sites (point-group symmetries). Angle-resolved XAS were employed[43] in strained CMR films to probe very tiny energy differences (shifts) at the Mn *K*-edge. However, in such measurements the two different absorption cross sections were detected[43] with the x-ray linear polarization of the electric field (incident beam) parallel and perpendicular to film surface. In interference RXS measurements,[23,24] the thin film is fixed and the detector is placed in two symmetric angles $\pm\phi_A$ about the $\sigma\rightarrow\pi'$ channel, where the ϕ_A is totally irrelevant to angle γ in the expression of a linear absorption coefficient $\mu(\gamma)$ that[43] takes into account the dichroic effect. In a forthcoming experiment, intensity difference $I(90°+\phi_A)-I(90°-\phi_A)$, RXS data will be compared to angle resolved[43] XAS measurements in order to separate the different components that give rise to nonzero RXS intensity difference at ~6.57 keV below the T_B.

IV. CONCLUSIONS

In summary, complementary x-ray diffraction and Mn *K*-edge resonant scattering measurements were employed to study the connection between EB mechanism and of the local scale structural distortion induced by epitaxial substrate strain around Mn ions in $[La_{2/3}Ca_{1/3}MnO_3(FM)/La_{1/3}Ca_{2/3}MnO_3(AF)]_{15}$ multilayers that exhibit EB below 80 K($=T_B$). It was observed that the T_B coincides with the temperature where the (in-plane) lattice parameter a_{ML} (Fig. 5) approaches the pseudocubic lattice constant observed[5] in the bulk form of the AF layers. The later might be responsible for: (i) the temperature of 90 K where the c/a ratio reaches its maximal value, (ii) the temperature where ξ^{-1} changes slope (Fig. 6), remaining constant up to ~70 K and then following the same temperature dependence as the axial c/a ratio (Fig. 5) up to 280 K. (iii) the temperature of 80 K, above which the RXS intensity difference becomes zero near the 6.57 keV postedge feature (Fig. 9). In contrast to the behavior of the postedge feature in Fig. 10, the energy shift of the main-edge feature does not vary linearly with temperature or the c/a-ratio. The former might be associated with a strain-driven rearrangement of Mn-O-Mn bonding angles around the T_B, whereas the second indicates that the width of the Mn-O pair distribution function fluctuates about the zero shift due to compositional modulation in the multilayer structure. Angle-resolved XAS measurements may reveal the origin of nonzero RXS intensity difference observed at 6.57 keV below the T_B.

ACKNOWLEDGMENTS

We thank the ESRF for provision of synchrotron x-ray beam time and I. Margiolaki and S. D. Brown for help with the ESRF experiments. Two of the authors (C.C. and N.M.) are indebted to D. Niarchos for provision of the pulsed laser deposition system.

*Author to whom correspondence should be addressed. Electronic address: christides@des.upatras.gr

[1] W. Kuch, L. I. Chelaru, F. Offi, J. Wang, M. Kotsugi, and J. Kirschner, Nat. Mater. **5**, 128 (2006); M. Blamire and B. Hickey, *ibid.* **5**, 87 (2006).
[2] I. Panagiotopoulos, C. Christides, M. Pissas, and D. Niarchos, Phys. Rev. B **60**, 485 (1999).
[3] N. Moutis, C. Christides, I. Panagiotopoulos, and D. Niarchos, Phys. Rev. B **64**, 094429 (2001).
[4] C. Christides, N. Moutis, Ph. Komninou, Th. Kehagias, and G. Nouet, J. Appl. Phys. **92**, 397 (2002).
[5] P. G. Radaelli, D. E. Cox, L. Capogna, S.-W. Cheong, and M. Marezio, Phys. Rev. B **59**, 14440 (1999).
[6] Y. Murakami, J. P. Hill, D. Gibbs, M. Blume, I. Koyama, M. Tanaka, H. Kawata, T. Arima, Y. Tokura, K. Hirota, and Y. Endoh, Phys. Rev. Lett. **81**, 582 (1998).
[7] J. H. Song, J. H. Park, K.-B. Lee, J. M. Lee, and Y. H. Jeong, Phys. Rev. B **66**, 020407 (2002).
[8] S. Ishihara and S. Maekawa, Rep. Prog. Phys. **65**, 561 (2002), for a review.
[9] M. Zimmermann, C. Nelson, Y.-J. Kim, J. Hill, D. Gibbs, H. Nakao, Y. Wakabayashi, Y. Murakami *et al.*, Phys. Rev. B **64**, 064411 (2001).
[10] A. M. Glazer, Acta Crystallogr., Sect. B: Struct. Crystallogr. Cryst. Chem. **28**, 3384 (1972); P. M. Woodward, *ibid.* **53**, 32 (1997); P. M. Woodward, *ibid.* **53**, 44 (1997).
[11] J. Kanamori, J. Appl. Phys. **31**, S14 (1960).
[12] S. Satpathy, Z. S. Popović, and F. R. Vukajlović, Phys. Rev. Lett. **76**, 960 (1996).
[13] J. Geck, P. Wochner, S. Kiele, R. Klingeler, A. Revcolevschi, M. v Zimmermann, B. Büchner, and P. Reutler, New J. Phys. **6**, 152 (2004), for a review.
[14] A. Yamasaki, M. Feldbacher, Y.-F. Yang, O. K. Andersen, and K. Held, Phys. Rev. Lett. **96**, 166401 (2006).
[15] I. S. Elfimov, V. I. Anisimov, and G. A. Sawatzky, Phys. Rev. Lett. **82**, 4264 (1999).
[16] M. Benfatto, Y. Joly, and C. R. Natoli, Phys. Rev. Lett. **83**, 636 (1999).
[17] M. v. Zimmermann, J. P. Hill, D. Gibbs, M. Blume, D. Casa, B. Keimer, Y. Murakami, Y. Tomioka, and Y. Tokura, Phys. Rev. Lett. **83**, 4872 (1999).
[18] M. v. Zimmermann, C. S. Nelson, J. P. Hill, D. Gibbs, M. Blume, D. Casa, B. Keimer, Y. Murakami, C. C. Kao, C. Venkataraman, T. Gog, Y. Tomioka, and Y. Tokura, Phys. Rev. B **64**, 195133 (2001).
[19] S. Grenier, J. P. Hill, D. Gibbs, K. J. Thomas, M. v. Zimmermann, C. S. Nelson, V. Kiryukhin, Y. Tokura, Y. Tomioka, D. Casa, T. Gog, and C. Venkataraman, Phys. Rev. B **69**, 134419 (2004).
[20] C. A. Marianetti, D. Morgan, and G. Ceder, Phys. Rev. B **63**, 224304 (2001).
[21] J. Herrero-Martin, J. García, G. Subías, J. Blasco, and M. C. Sánchez, Phys. Rev. B **70**, 024408 (2004).
[22] R. K. Zheng, G. Li, A. N. Tang, Y. Yang, W. Wang, X. G. Li, Z. D. Wang, and H. C. Ku, Appl. Phys. Lett. **83**, 5250 (2003).
[23] H. Ohsumi, Y. Murakami, T. Kiyama, H. Nakao, M. Kubota, Y. Wakabayashi, Y. Konishi, M. Izumi, M. Kawasaki, and Y. Tokura, J. Phys. Soc. Jpn. **72**, 1006 (2003).
[24] Y. Wakabayashi, H. Sawa, M. Nakamura, M. Izumi, and K. Miyano, Phys. Rev. B **69**, 144414 (2004).
[25] T. Kiyama, Y. Wakabayashi, H. Nakao, H. Ohsumi, Y. Murakami, M. Izumi, M. Kawasaki, and Y. Tokura, J. Phys. Soc. Jpn. **72**, 785 (2003).
[26] A. J. Millis, Nature (London) **392**, 147 (1998).
[27] C. J. Lu, Z. L. Wang, C. Kwon, and Q. X. Jia, J. Appl. Phys. **88**, 4032 (2000).
[28] S. D. Brown, L. Bouchenoire, D. Bowyer, J. Kervin, D. Laundy, M. J. Longfield, D. Mannix, D. F. Paul *et al.*, J. Synchrotron Radiat. **8**, 1172 (2001).
[29] A. de Andrés, J. Rubio, G. Castro, S. Taboada, J. L. Martínez, and J. M. Colino, Appl. Phys. Lett. **83**, 713 (2003).
[30] J. Mattson, R. Bhadra, J. B. Ketterson, M. Brodsky, and M. Grimsditch, J. Appl. Phys. **67**, 2873 (1990).
[31] C. Dubourdieu, M. Rosina, H. Roussel, F. Weiss, J. P. Sénateur, and J. L. Hodeau, Appl. Phys. Lett. **79**, 1246 (2001).
[32] O. Morán, M. E. Gomez, J. G. Ramirez, T. Swartz, D. Fuchs, R. Hott, and R. Schneider, J. Appl. Phys. **97**, 10K116 (2005).
[33] J.-H. Song, K. K. Kim, Y. J. Oh, H.-J. Jung, W. K. Choi, J. H. Song, and D.-K. Choi, J. Vac. Sci. Technol. A **A 18**, 5, 2437 (2000).
[34] Q. Huang, A. Santoro, J. W. Lynn, R. W. Erwin, J. A. Borchers, J. L. Peng, K. Ghosh, and R. L. Greene, Phys. Rev. B **58**, 2684 (1998).
[35] M. Ohring, in *Materials Science of Thin Films*, 2nd ed. (Academic Press, New York, 2002), pp. 732, 777.
[36] Y. Lu, J. Klein, F. Herbstritt, J. B. Philipp, A. Marx, and R. Gross, Phys. Rev. B **73**, 184406 (2006); Y. Lu, J. Klein, C. Hoefener, B. Wiedenhorst, J. B. Philipp, F. Herbstritt, A. Marx, L. Alff, and R. Gross, *ibid.* **62**, 15806 (2000).
[37] Y. P. Lee, S. Y. Park, Y. H. Hyun, J. B. Kim, V. G. Prokhorov, V. A. Komashko, and V. L. Svetchnikov, Phys. Rev. B **73**, 224413 (2006).
[38] L. M. Berndt, V. Balbarin, and Y. Suzuki, Appl. Phys. Lett. **77**, 2903 (2000).
[39] D. Sander, Rep. Prog. Phys. **62**, 809 (1999).
[40] O. Hjortstam, K. Baberschke, J. M. Wills, B. Johansson, and O. Eriksson, Phys. Rev. B **55**, 15026 (1997).
[41] B. Ravel, S. Grenier, H. Renevier, and C.-B. Eom, J. Synchrotron Radiat. **8**, 384 (2001).
[42] F. Bridges, C. H. Booth, G. H. Kwei, J. J. Neumeier, and G. A. Sawatzky, Phys. Rev. B **61**, R9237 (2000).
[43] N. M. Souza-Neto, A. Y. Ramos, H. C. N. Tolentino, E. Favre-Nicolin, and L. Ranno, Phys. Rev. B **70**, 174451 (2004).
[44] F. Bridges, C. H. Booth, M. Anderson, G. H. Kwei, J. J. Neumeier, J. Snyder, J. Mitchell, J. S. Gardner, and E. Brosha, Phys. Rev. B **63**, 214405 (2001).
[45] J. García, M. C. Sánchez, G. Sibías, and J. Blasco, J. Phys.: Condens. Matter **13**, 3229 (2001).
[46] G. Subías, J. García, M. G. Proietti, and J. Blasco, Phys. Rev. B **56**, 8183 (1997).
[47] V. E. Dmitrienco, K. Ishiba, A. Kirfel, and E. N. Ovchinnikova, Acta Crystallogr., Sect. A: Found. Crystallogr. **56**, 481 (2005); V. E. Dmitrienco, *ibid.* **39**, 29 (1983); **40**, 89 (1984).
[48] D. H. Templeton and L. K. Templeton, Acta Crystallogr., Sect. A: Cryst. Phys., Diffr., Theor. Gen. Crystallogr. **36**, 237 (1980).
[49] A. Yu. Ignatov, N. Ali, and S. Khalid, Phys. Rev. B **64**, 014413 (2001).
[50] D. Cao, F. Bridges, D. C. Worledge, C. H. Booth, and T. Geballe, Phys. Rev. B **61**, 11373 (2000).
[51] C. Brouder, J. Phys.: Condens. Matter **2**, 701 (1990).